

DOI: 10.7511/jslx20221106001

基于改进 Reddy 型三阶剪切变形理论的弹性 地基上 FG-CNTRC 板屈曲无网格分析

许建文¹, 严世涛², 彭林欣³, 陈卫^{*3,4}

(1. 广西新发展交通集团有限公司, 南宁 530004; 2. 广西交通职业技术学院, 南宁 530004;
3. 广西大学 土木建筑工程学院, 南宁 530004; 4. 南华大学 土木工程学院, 衡阳 421001)

摘要:针对含碳纳米管转向的 Pasternak 地基上功能梯度碳纳米管增强复合材料 FG-CNTRC(functionally graded carbon nanotube-reinforced composite)板的屈曲问题,提出了一种基于改进 Reddy 型三阶剪切变形理论 TSDT(third-order shear deformation theory)和移动最小二乘近似 MLS(moving-least square)的无网格分析模型。该模型避免了无网格法第二类边界条件的施加困难问题,且能够满足中厚/厚板的自由表面条件,无需额外引入剪切修正因子。基于最小势能原理推导了弹性地基上 FG-CNTRC 板的无网格屈曲控制方程,采用完全转换法处理本质边界条件。通过基准算例验证了本文方法的收敛性及有效性,讨论了碳纳米管的转向角、体积分数、分布形式、地基系数、宽厚比和边界条件等对 FG-CNTRC 板临界屈曲荷载的影响。

关键词:改进 Reddy 型三阶剪切变形理论;功能梯度碳纳米管增强复合材料板;Pasternak 地基;临界屈曲荷载;移动最小二乘近似

中图分类号: TU339; O343.9

文献标志码: A

文章编号: 1007-4708(2024)03-0572-10

1 引言

碳纳米管 CNTs(carbon nanotubes)是一种新型的先进材料,由细长的碳柱组成。许多试验和理论研究表明, CNTs 具有高强度、高刚度和低密度等特性,通过添加少量 CNTs 就可以提高聚合物复合材料的力学和热-电性能^[1,2]。为推广其应用,诸多学者开展了 CNTs 增强复合材料梁、板、壳线性弯曲、自由振动和屈曲等力学性能的研究^[3-8]。

受功能梯度材料 FGMs(functionally graded materials)启发,研究者将 CNTs 以特定的形式排布而形成了功能梯度碳纳米管增强复合材料 FG-CNTRC(functionally graded carbon nanotube reinforced composite)的概念。Shen^[9]率先基于三阶剪切变形理论 TSDT(third-order shear deformation theory)和二次摄动法分析了 FG-CNTRC 板在横向均布或正弦分布荷载作用下的非线性弯曲问

题。Shen 等^[10]同样基于 TSDT,采用二次摄动法求解了 FG-CNTRC 板的热屈曲及后屈曲问题。Yas 等^[11]结合一阶剪切变形理论 FSDT(first-order shear deformation theory)和广义微分求积法 GDQM(generalized differential quadrature method)求解了 Pasternak 地基上 FG-CNTRC 梁的自由振动与屈曲问题。Wattanasakulpong 等^[12,13]在不同横向剪切变形理论框架下,采用 Navier 解答给出了简支边界条件下 Pasternak 地基上 FG-CNTRC 梁、板线性弯曲、自由振动及屈曲的解析解。Zhang 等^[14]基于 FSDT,采用改进的移动最小二乘-瑞兹法 IMLS-Ritz(improved moving least squares-Ritz)对 winkler 地基上的 FG-CNTRC 板屈曲问题进行了分析。

无网格法作为数值算法的一种,具有收敛快和计算精度高等特点。其形函数形成只依赖于节点信息,易构造高阶光滑近似(应力计算结果光滑),在板

收稿日期: 2022-11-06; 修改稿收到日期: 2022-12-21.

基金项目: 国家自然科学基金(12162004; 11562001); 广西高校中青年骨干教师科研基础能力提升项目(2022KY1140)资助。

作者简介: 陈卫* (1991-), 男, 博士, 讲师, 硕士生导师(Email: w.chen@st.gxu.edu.cn).

引用本文: 许建文, 严世涛, 彭林欣, 等. 基于改进 Reddy 型三阶剪切变形理论的弹性地基上 FG-CNTRC 板屈曲无网格分析[J]. 计算力学学报, 2024, 41(3): 572-581.

XU Jian-wen, YAN Shi-tao, PENG Lin-xin, et al. Meshless buckling analysis of FG-CNTRC plate on elastic foundation based on improved Reddy type third-order shear deformation theory[J]. Chinese Journal of Computational Mechanics, 2024, 41(3): 572-581.

壳数值计算分析方面具有天然优势^[15]。当梁和板壳变很薄时,可能会出现剪切锁死现象。基于移动最小二乘近似的无网格法,可通过提高形函数中基函数的阶次或扩大影响域来缓解甚至完全避免剪切锁死现象^[16]。但无网格法在施加第二类边界条件,即挠度的偏导($\partial w_0/\partial x, \partial w_0/\partial y$)时存在一定困难,因此绝大多数无网格法文献均是结合 FSDT 对中厚板的线性弯曲、自由振动与屈曲等力学性能进行研究^[17-23],该方法无法满足中厚板的自由表面条件,需人工引入剪切修正因子。Vu 等^[24]假设 $w_0(x, y) = w_b(x, y) + w_s(x, y)$, $\phi_x = -\partial w_b(x, y)/\partial x$ 和 $\phi_y = -\partial w_b(x, y)/\partial y$ 在 FSDT 的基础上提出了简单的 FSDT,结合移动克里金 MK (moving kriging) 插值对 FGM 板进行了线性弯曲与自由振动分析。该方法需借助流函数列式技术,即在边界节点处内置对应的临近节点来施加第二类边界条件,使得计算成本大大增加,降低了计算效率。Selim 等^[25]将 Reddy 的 TSDT^[26]进行了改进,假设 $\Psi_x = \varphi_x + \partial w_0/\partial x$, $\Psi_y = \varphi_y + \partial w_0/\partial y$,即将广义位移场的五个自由度变量转化为七个自由度变量,结合再生核粒子-瑞兹法 kp-Ritz (reproducing kernel particle method-Ritz) 研究了 FG-CNTRC 中厚/厚板的自由振动问题。此后, Selim 等^[27-29]采用改进 Reddy 的 TSDT,结合无网格法对功能梯度及 CNTRC 压电板的主动振动控制和 CNTs 增强层合板的自由振动问题进行了研究。

综上所述,基于 TSDT 研究 FG-CNTRC 板的屈曲性能鲜见相关报道,且讨论 CNTs 转向角的文献较为罕见^[6,30]。本文将基于改进 Reddy 型 TSDT,结合 MLS 近似的无网格法对 Pasternak 地基上 FG-CNTRC 板的屈曲性能进行研究。详细讨论 CNTs 的转向角、体积分数、分布形式、地基系数及边界条件等对临界屈曲荷载的影响。

2 Pasternak 地基上 FG-CNTRC 板

如图 1(a) 所示的 Pasternak 地基 FG-CNTRC 板,板的长、宽和高分别记为 a, b 和 h 。CNTs 作为增强体,通过引入 CNTs 的效能参数,根据广义混合律将 CNTs 以功能梯度方式嵌入到基体中

$$\begin{cases} E_{11} = \eta_1 V_{\text{CNT}} E_{11}^{\text{CNT}} + V_m E^m \\ \eta_2 = \frac{V_{\text{CNT}}}{E_{22}^{\text{CNT}}} + \frac{V_m}{E^m} \\ E_{22} = \eta_2 E_{22}^{\text{CNT}} + V_m E^m \\ \eta_3 = \frac{V_{\text{CNT}}}{G_{12}^{\text{CNT}}} + \frac{V_m}{G^m} \\ G_{12} = \eta_3 G_{12}^{\text{CNT}} + V_m G^m \end{cases} \quad (1)$$

式中 E_{11}, E_{22} 和 G_{12} 分别为 CNTRC 板的等效杨氏模量和剪切模量; $E_{11}^{\text{CNT}}, E_{22}^{\text{CNT}}$ 和 G_{12}^{CNT} 分别为碳纳米管的杨氏模量和剪切模量; E^m 和 G^m 分别为基体的杨氏模量和剪切模量; V_{CNT} 和 V_m 分别为碳纳米管和基体的体积分数,且 $V_{\text{CNT}} + V_m = 1$; n_j ($j = 1, 2, 3$) 为碳纳米管的效能参数; FG-CNTRC 泊松比和质量密度可定义为

$$\nu_{12} = V_{\text{CNT}} \nu_{12}^{\text{CNT}} + V_m \nu^m \quad (2)$$

$$\rho = V_{\text{CNT}} \rho^{\text{CNT}} + V_m \rho^m \quad (3)$$

式中 ν_{12} 和 ρ 分别为 CNTRC 的等效泊松比和等效密度, ν_{12}^{CNT} 和 ν^m 为碳纳米管和基体的泊松比, ρ^{CNT} 和 ρ^m 为碳纳米管和基体的质量密度。

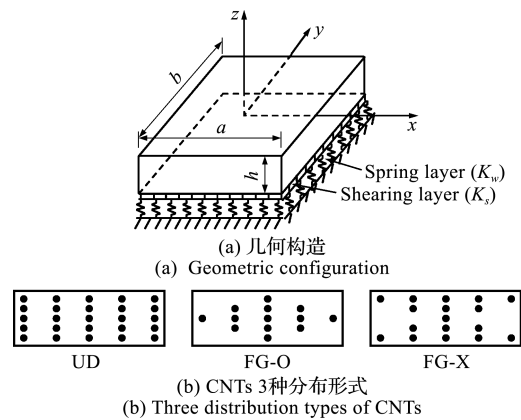


图 1 Pasternak 地基上 FG-CNTRC 板的等效模型
Fig. 1 Equivalent model of FG-CNTRC plate on pasternak foundation

本文考虑常见的 3 种碳纳米管分布形式 (UD 型、FG-O 型和 FG-X 型), 如图 1(b) 所示, 相应的体积率表达式为

$$V_{\text{CNT}} = \begin{cases} V_{\text{CNT}}^* & (\text{UD}) \\ 2(1 - 2|z|/h)V_{\text{CNT}}^* & (\text{FG-O}) \\ 4|z|/h V_{\text{CNT}}^* & (\text{FG-X}) \end{cases} \quad (4)$$

$$\text{式中 } V_{\text{CNT}}^* = \frac{w_{\text{CNT}}}{w_{\text{CNT}} + (\rho^{\text{CNT}}/\rho^m)(1 - w_{\text{CNT}})} \quad (5)$$

式中 w_{CNT} 为碳纳米管的质量分数, ρ^{CNT} 和 ρ^m 为碳纳米管和基体的密度。

Pasternak 地基模型^[31]为

$$q_e(x, y) = K_w w(x, y) - K_s \nabla^2 w(x, y) \quad (6)$$

式中 K_w 为弹性地基系数, K_s 为地基剪切模量, $\nabla^2 = \partial^2/x^2 + \partial^2/y^2$; 当 $K_s = 0$ 时, Pasternak 地基模型则简化为 Winkler 模型。

3 弹性地基 FG-CNTRC 板的无网格列式

3.1 形函数

假设 FG-CNTRC 板中面节点总数为 n , 由移

动最小二乘近似^[32]可得板第 I 个节点的形函数

$$N_I(x, y) = \mathbf{q}^T(x, y) \mathbf{B}^{-1}(x, y) \mathbf{q}(x_I, y_I) \times \bar{\omega}(x - x_I, y - y_I) \quad (7)$$

式中 $\mathbf{B}(x, y) = \sum_{I=1}^n \bar{\omega}(x - x_I, y - y_I) \mathbf{q}(x_I, y_I) \times \mathbf{q}^T(x, y)$, $\mathbf{q}^T(x, y) = [1, x, y, x^2, y^2, xy, y^2]$ 为二维空间单项式基函数。 $\bar{\omega}$ 取三次样条权函数

$$\omega(x - x_I) = \begin{cases} 2/3 - 4r^2 + 4r^3 & (r \leq 1/2) \\ 4/3 - 4r + 4r^2 - 4r^3/3 & (1/2 < r \leq 1) \\ 0 & (r > 1) \end{cases} \quad (8)$$

因此,域内函数 $u(\mathbf{x})$ 的近似函数 $u^h(\mathbf{x})$ 可表示为

$$u^h(\mathbf{x}) = \sum_{I=1}^n N_I(\mathbf{x}, y) u_I \quad (9)$$

式中 u_I 为第 I 个节点的非真实位移(节点参数)。

3.2 总能量泛函

根据 Reddy's 三阶剪切变形理论^[26],含五个自由变量的板位移场 $\mathbf{U} = (u, v, w)^T$ 可表示为

$$\begin{cases} u(x, y, z) = u_0(x, y) + z\varphi_x(x, y) + cz^3(\varphi_x + \partial w/\partial x) \\ v(x, y, z) = v_0(x, y) + z\varphi_y(x, y) + cz^3(\varphi_y + \partial w/\partial y) \\ w(x, y, z) = w_0(x, y) \end{cases} \quad (10)$$

式中 $(u_0, v_0, w_0)^T$ 为板中面任意一点在 x, y 和 z 方向的位移, φ_x 和 φ_y 分别为绕 y 轴和 x 轴的转动, $c = -4/3h^2$ 。根据文献[25, 30],假设 $\Psi_x = \varphi_x + \partial w_0/\partial x$, $\Psi_y = \varphi_y + \partial w_0/\partial y$,式(10)可改写为含七个自由度变量的位移场

$$\begin{cases} u(x, y, z) = u_0(x, y) + z\varphi_x(x, y) + cz^3\Psi_x(x, y) \\ v(x, y, z) = v_0(x, y) + z\varphi_y(x, y) + cz^3\Psi_y(x, y) \\ w(x, y, z) = w_0(x, y) \end{cases} \quad (11)$$

根据几何方程,板的内应变和剪切应变分别为

$$\boldsymbol{\varepsilon} = \{\varepsilon_x \ \varepsilon_y \ \gamma_{xy}\}^T = \boldsymbol{\varepsilon}_0 + z\boldsymbol{\kappa}_1 + z^3\boldsymbol{\kappa}_2 \quad (12)$$

$$\boldsymbol{\gamma} = \{\gamma_{yz} \ \gamma_{xz}\}^T = \boldsymbol{\varepsilon}_s + z^2\boldsymbol{\kappa}_s \quad (13)$$

式中 $\boldsymbol{\varepsilon}_0 = \{u_{0,x} \ v_{0,y} \ u_{0,y} + v_{0,x}\}^T$
 $\boldsymbol{\kappa}_1 = \{\varphi_{x,x} \ \varphi_{y,y} \ \varphi_{x,y} + \varphi_{y,x}\}^T$
 $\boldsymbol{\kappa}_2 = c\{\Psi_{x,x} \ \Psi_{y,y} \ \Psi_{x,y} + \Psi_{y,x}\}^T$
 $\boldsymbol{\varepsilon}_s = \{\varphi_x + w_{0,x} \ \varphi_y + w_{0,y}\}^T$
 $\boldsymbol{\kappa}_s = 3c\{\Psi_x \ \Psi_y\}^T$

正交各向异性材料的本构关系为

$$\begin{Bmatrix} \sigma_x \\ \sigma_y \\ \tau_{xy} \\ \tau_{xz} \\ \tau_{yz} \end{Bmatrix} = \begin{bmatrix} \bar{Q}_{11} & \bar{Q}_{12} & \bar{Q}_{16} & 0 & 0 \\ \bar{Q}_{12} & \bar{Q}_{22} & \bar{Q}_{26} & 0 & 0 \\ \bar{Q}_{16} & \bar{Q}_{26} & \bar{Q}_{66} & 0 & 0 \\ 0 & 0 & 0 & \bar{Q}_{55} & \bar{Q}_{45} \\ 0 & 0 & 0 & \bar{Q}_{45} & \bar{Q}_{44} \end{bmatrix} \begin{Bmatrix} \varepsilon_x \\ \varepsilon_y \\ \gamma_{xy} \\ \gamma_{xz} \\ \gamma_{yz} \end{Bmatrix} \quad (14)$$

式中 \bar{Q}_{ij} 为全局 x, y 坐标系中弹性矩阵的分量,可通过以下坐标转换方程变换得到

$$[\bar{\mathbf{Q}}] = [\mathbf{T}][\mathbf{Q}][\mathbf{T}]^T \quad (15)$$

式中

$$\mathbf{T} = \begin{bmatrix} m^2 & n^2 & -2mn & 0 & 0 \\ n^2 & m^2 & 2mn & 0 & 0 \\ mn & -mn & m^2 - n^2 & 0 & 0 \\ 0 & 0 & 0 & m & -n \\ 0 & 0 & 0 & n & m \end{bmatrix}$$

$$\mathbf{Q} = \begin{bmatrix} Q_{11}(z) & Q_{12}(z) & 0 & 0 & 0 \\ Q_{12}(z) & Q_{22}(z) & 0 & 0 & 0 \\ 0 & 0 & Q_{66}(z) & 0 & 0 \\ 0 & 0 & 0 & Q_{55}(z) & 0 \\ 0 & 0 & 0 & 0 & Q_{44}(z) \end{bmatrix}$$

式中 $m = \cos\theta, n = \sin\theta; \theta$ 为 CNTs 在全局坐标系 $x-y$ 面内绕着 x 轴逆时针旋转的角度, Q_{ij} 为碳纳米管横向分布时 FG-CNTRC 板物理关系矩阵,表达式为

$$Q_{11} = \frac{E_{11}}{1 - \nu_{12}\nu_{21}}, Q_{22} = \frac{E_{22}}{1 - \nu_{12}\nu_{21}}, Q_{12} = \frac{\nu_{21}E_{11}}{1 - \nu_{12}\nu_{21}}$$

$$Q_{66} = G_{12}, Q_{44} = G_{23}, Q_{55} = G_{13}, \nu_{21} = \frac{E_{22}}{E_{11}}\nu_{12} \quad (16)$$

式中 E_{11} 和 E_{22} 分别为 1 方向和 2 方向上的杨氏模量, G_{12}, G_{31} 和 G_{23} 分别为 1-2, 1-3 和 2-3 平面的剪切模量, ν_{ij} 为应力在 i 方向作用时 j 方向的横向应变泊松比。

FG-CNTRC 板的应变能为

$$U_p = \frac{1}{2} \int_{\Omega} \boldsymbol{\varepsilon}^T \mathbf{S} \boldsymbol{\varepsilon} d\Omega \quad (17)$$

式中

$$\boldsymbol{\varepsilon} = \begin{Bmatrix} \boldsymbol{\varepsilon}_0 \\ \boldsymbol{\kappa}_1 \\ \boldsymbol{\kappa}_2 \\ \boldsymbol{\varepsilon}_s \\ \boldsymbol{\kappa}_s \end{Bmatrix}, \mathbf{S} = \begin{bmatrix} \mathbf{A} & \mathbf{B} & \mathbf{E} & \mathbf{0} & \mathbf{0} \\ \mathbf{B} & \mathbf{D} & \mathbf{F} & \mathbf{0} & \mathbf{0} \\ \mathbf{E} & \mathbf{F} & \mathbf{H} & \mathbf{0} & \mathbf{0} \\ \mathbf{0} & \mathbf{0} & \mathbf{0} & \mathbf{A}^s & \mathbf{D}^s \\ \mathbf{0} & \mathbf{0} & \mathbf{0} & \mathbf{D}^s & \mathbf{F}^s \end{bmatrix}$$

$$(A_{ij}, B_{ij}, D_{ij}, E_{ij}, F_{ij}, H_{ij}) =$$

$$\int_{-h/2}^{h/2} \bar{Q}_{ij}(1, z, z^2, z^3, z^4, z^6) dz \quad (i, j = 1, 2, 6)$$

$$(A_{ij}^s, D_{ij}^s, F_{ij}^s) = \int_{-h/2}^{h/2} \bar{Q}_{ij}(1, z^2, z^4) dz \quad (i, j = 4, 5)$$

由式(6),可得 Pasternak 地基势能一阶变分为

$$\delta U_e = \int_{\Omega} q_e \delta w_p d\Omega = \int_{\Omega} \left\{ K_w w_p - K_s \left(\frac{\partial^2 w_p}{\partial x^2} + \frac{\partial^2 w_p}{\partial y^2} \right) \right\} \delta w_p d\Omega \quad (18)$$

对 FG-CNTRC 板施加如图 2 所示面内荷载作用时的势能为

$$W_g = \int_{\Omega} \begin{bmatrix} \frac{\partial w}{\partial x} & \frac{\partial w}{\partial y} \end{bmatrix} \begin{bmatrix} R_x & R_{xy} \\ R_{xy} & R_y \end{bmatrix} \begin{bmatrix} \frac{\partial w}{\partial x} \\ \frac{\partial w}{\partial y} \end{bmatrix} d\Omega \quad (19)$$

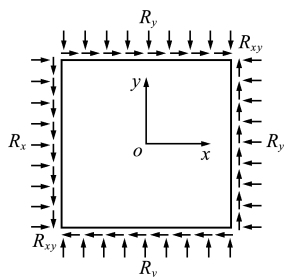


图2 面内荷载作用下的 FG-CNTRC 板
Fig.2 FG-CNTRC plate subjected to in-plane loads

将式(17~19)进行叠加,则得 Pasternak 地基上 FG-CNTRC 板屈曲时的总势能泛函为

$$\Pi = U_p + U_e - W_g \quad (20)$$

3.3 控制方程

对 FG-CNTRC 板的节点位移及转角进行离散,利用式(9)近似得到

$$u_0^h = \begin{bmatrix} u_0^h \\ v_0^h \\ w_0^h \\ \varphi_x^h \\ \varphi_y^h \\ \Psi_x^h \\ \Psi_y^h \end{bmatrix} = \sum_{l=1}^n N_l(x) u_l = \sum_{l=1}^n N_l(x) \begin{bmatrix} u_l \\ v_l \\ w_l \\ \varphi_{xl} \\ \varphi_{yl} \\ \Psi_{xl} \\ \Psi_{yl} \end{bmatrix} \quad (21)$$

将式(21)代入式(20),根据最小势能原理, $\delta\Pi = 0$, 可得

$$(\mathbf{K} - \mathbf{G})\mathbf{U} = 0 \quad (22)$$

式中

$$\mathbf{K} = \mathbf{K}_p + \mathbf{K}_e$$

$$\mathbf{K}_p = \int_{\Omega} \begin{bmatrix} \mathbf{B}_m^T \\ \mathbf{B}_{b1}^T \\ \mathbf{B}_{b2}^T \\ \mathbf{B}_{s1}^T \\ \mathbf{B}_{s2}^T \end{bmatrix} \begin{bmatrix} \mathbf{A} & \mathbf{B} & \mathbf{E} & \mathbf{0} & \mathbf{0} \\ \mathbf{B} & \mathbf{D} & \mathbf{F} & \mathbf{0} & \mathbf{0} \\ \mathbf{E} & \mathbf{F} & \mathbf{H} & \mathbf{0} & \mathbf{0} \\ \mathbf{0} & \mathbf{0} & \mathbf{0} & \mathbf{A}_s & \mathbf{D}_s \\ \mathbf{0} & \mathbf{0} & \mathbf{0} & \mathbf{D}_s & \mathbf{F}_s \end{bmatrix} \begin{bmatrix} \mathbf{B}_m \\ \mathbf{B}_{b1} \\ \mathbf{B}_{b2} \\ \mathbf{B}_{s1} \\ \mathbf{B}_{s2} \end{bmatrix} d\Omega$$

$$\mathbf{K}_e = \int_{\Omega} [0, 0, N_I, 0, 0, 0, 0]^T [0, 0, K_w N_I - K_s(N_{I,xx} + N_{I,yy}), 0, 0, 0, 0] d\Omega$$

$$\mathbf{G} = \int_{\Omega} \mathbf{G}_I^T \bar{\mathbf{N}} \mathbf{G}_J d\Omega$$

式中

$$\mathbf{B}_m = \begin{bmatrix} N_{I,x} & 0 & 0 & 0 & 0 & 0 & 0 \\ 0 & N_{I,y} & 0 & 0 & 0 & 0 & 0 \\ N_{I,y} & N_{I,x} & 0 & 0 & 0 & 0 & 0 \end{bmatrix}$$

$$\mathbf{B}_{b1} = \begin{bmatrix} 0 & 0 & 0 & N_{I,x} & 0 & 0 & 0 \\ 0 & 0 & 0 & 0 & N_{I,y} & 0 & 0 \\ 0 & 0 & 0 & N_{I,y} & N_{I,x} & 0 & 0 \end{bmatrix}$$

$$\mathbf{B}_{b2} = c \begin{bmatrix} 0 & 0 & 0 & 0 & 0 & N_{I,x} & 0 \\ 0 & 0 & 0 & 0 & 0 & 0 & N_{I,y} \\ 0 & 0 & 0 & 0 & 0 & N_{I,y} & N_{I,x} \end{bmatrix}$$

$$\mathbf{B}_{s1} = \begin{bmatrix} 0 & 0 & N_{I,x} & N_I & 0 & 0 & 0 \\ 0 & 0 & N_{I,y} & 0 & N_I & 0 & 0 \end{bmatrix}$$

$$\mathbf{B}_{s2} = 3c \begin{bmatrix} 0 & 0 & 0 & 0 & 0 & N_I & 0 \\ 0 & 0 & 0 & 0 & 0 & 0 & N_I \end{bmatrix}$$

$$\mathbf{G}_I = \begin{bmatrix} 0 & 0 & N_{I,x} & 0 & 0 & 0 & 0 \\ 0 & 0 & N_{I,y} & 0 & 0 & 0 & 0 \end{bmatrix}, \bar{\mathbf{N}} = \begin{bmatrix} R_x & R_{xy} \\ R_{xy} & R_y \end{bmatrix}$$

3.4 本质边界条件处理

基于移动最小二乘近似得到的形函数不满足 Kronecker 条件,其未知量不是节点的真实位移,本文采用 Chen 等^[33]提出的完全转换法处理本质边界条件。

根据式(9), $\bar{\mathbf{U}}(\mathbf{x})$ 可以通过 $\mathbf{U}^h(\mathbf{x})$ 近似如下

$$\bar{\mathbf{U}}(\mathbf{x}) \approx \mathbf{U}^h(\mathbf{x}) = \sum_{l=1}^n N_l(\mathbf{x}) \mathbf{U}_l = \mathbf{A} \mathbf{U} \quad (23)$$

式中 $\bar{\mathbf{U}}(\mathbf{x}) = \{\bar{U}_1(\mathbf{x}), \bar{U}_2(\mathbf{x}), \dots, \bar{U}_n(\mathbf{x})\}^T$

$$\mathbf{U}^h(\mathbf{x}) = \{U_1^h(\mathbf{x}), U_1^h(\mathbf{x}), \dots, U_n^h(\mathbf{x})\}^T$$

U_l 为节点参数

$$\mathbf{U} = \{U_1, U_2, \dots, U_n\}^T$$

$$\mathbf{A} = \begin{bmatrix} N_1(x_1) & N_2(x_1) & \dots & N_n(x_1) \\ N_1(x_2) & N_2(x_2) & \dots & N_n(x_2) \\ \vdots & \vdots & \ddots & \vdots \\ N_1(x_n) & N_2(x_n) & \dots & N_n(x_n) \end{bmatrix}$$

式(23)两边同时乘以 \mathbf{A}^{-1} 得到

$$\mathbf{A}^{-1} \bar{\mathbf{U}} = \mathbf{A}^{-1} \mathbf{A} \mathbf{U} \quad (24)$$

令 $\mathbf{T} = \mathbf{A}^{-1}$, 变换式(24)有

$$\mathbf{U} = \mathbf{T} \bar{\mathbf{U}} \quad (25)$$

于是有

$$(\mathbf{K} - \mathbf{G})\mathbf{U} = 0 \Rightarrow (\mathbf{T}^T \mathbf{K} \mathbf{T} - \mathbf{T}^T \mathbf{G} \mathbf{T}) \bar{\mathbf{U}} = 0 \quad (26)$$

令 $\bar{\mathbf{K}} = \mathbf{T}^T \mathbf{K} \mathbf{T}, \bar{\mathbf{G}} = \mathbf{T}^T \mathbf{G} \mathbf{T}$, 则可得到修正后的控制方程为

$$(\bar{\mathbf{K}} - \bar{\mathbf{G}}) \bar{\mathbf{U}} = 0 \quad (27)$$

设 $R_x = c_1 R_y, R_x = c_2 R_{xy}$ (c_1 和 c_2 为常数), 把 R_x 从 $\bar{\mathbf{G}}$ 中提出来, 则有

$$(\bar{\mathbf{K}} - R_x \hat{\mathbf{G}}) \bar{\mathbf{U}} = 0 \quad (28)$$

解这个特征值方程, 可得 Pasternak 地基上 FG-CNTRC 板的临界屈曲荷载。

4 算例分析

本文算例均采用方形影响域, 影响域大小定义为 $h_x = \lambda \times I_x, h_y = \lambda \times I_y$, h_x 和 h_y 分别为影响域 x 和 y 向长度, I_x 和 I_y 分别为 x 和 y 向相邻节点间距, 系数 $\lambda = 4.0$ 。高斯节点数为 4×4 。板由单壁

碳纳米管 SWCNTs (single-walled carbon nanotubes) 增强体和聚酰亚胺薄膜基体 PmPV (poly-cp-vinylene) 混合组成, SWCNTs 几何尺寸为, 长度 $L = 9.26 \text{ nm}$, $R = 0.68 \text{ nm}$, $h = 0.067 \text{ nm}$, 其他相关材料参数列入表 1 和表 2。临界屈曲荷载及地基系数无量纲公式为

$$\bar{N}_{cr} = N_{cr} b^2 / E^m h^3, k_w = K_w b^4 / D_m$$

$$k_s = K_s b^2 / D_m, D_m = E^m h^3 / [12(1 - (\nu^m)^2)]$$

数值试验中 FG-CNTRC 板结构考虑如下三种边界条件。

(1) 固支边界(C)

当 $x = \pm a/2$ 时

$$v = w = \varphi_x = \varphi_y = \Psi_x = \Psi_y = 0$$

当 $y = \pm b/2$ 时

$$u = w = \varphi_x = \varphi_y = \Psi_x = \Psi_y = 0$$

(2) 简支边界(S)

当 $x = \pm a/2$ 时, $v = w = \varphi_y = \Psi_y = 0$

当 $y = \pm b/2$ 时, $u = w = \varphi_x = \Psi_x = 0$

(3) 自由边界(F), 没有限制。

表 1 材料参数

Tab. 1 Properties of material

| Parameters | Matrix | CNTs |
|----------------------------|-----------------|--|
| Poisson's ratio | $\nu^m = 0.34$ | $\nu_{12}^{\text{CNT}} = 0.175$ |
| Density/kg·m ⁻³ | $\rho^m = 1150$ | $\rho^{\text{CNT}} = 1400$ |
| Young's modulus/GPa | $E^m = 2.1$ | $E_{11}^{\text{CNT}} = 5646.6$ $E_{22}^{\text{CNT}} = 7080$ |
| Shear modulus/GPa | — | $G_{12}^{\text{CNT}} = 1944.5$ |

表 2 与体积分数对应 CNTs 的效能参数

Tab. 2 Efficiency parameters of CNTs corresponding to volume fraction

| Efficiency parameters | V_{CNT}^* | | |
|-----------------------|--------------------|-------|-------|
| | 0.11 | 0.14 | 0.17 |
| η_1 | 0.149 | 0.150 | 0.149 |
| η_2 | 0.934 | 0.941 | 1.381 |
| η_3 | 0.934 | 0.941 | 1.381 |

表 4 单压弹性地基上四边简支 FG-CNTRC 方板无量纲临界屈曲荷载

Tab. 4 Dimensionless critical buckling loads of simply supported FG-CNTRC square plate on elastic foundation under uniaxial compression

| V_{CNT}^* | Type | $(k_w, k_s) = (0, 0)$ | | | $(k_w, k_s) = (100, 0)$ | | | $(k_w, k_s) = (100, 50)$ | | |
|--------------------|------|-----------------------|----------------------|---------|-------------------------|----------------------|---------|--------------------------|----------------------|---------|
| | | TSDT ^[13] | SSDT ^[13] | Present | TSDT ^[13] | SSDT ^[13] | Present | TSDT ^[13] | SSDT ^[13] | Present |
| | | 0.11 | UD | 20.6814 | 20.7286 | 20.6724 | 21.7080 | 21.7552 | 21.6990 | 31.8401 |
| | FG-O | 14.4990 | 14.4515 | 14.4429 | 15.5256 | 15.4781 | 15.4695 | 25.6577 | 25.6102 | 25.6016 |
| | FG-X | 24.5864 | 24.3943 | 24.2290 | 25.3130 | 25.4209 | 25.2556 | 35.4451 | 35.5531 | 35.3876 |
| 0.14 | UD | 23.3559 | 23.4229 | 23.3397 | 24.3825 | 24.4495 | 24.3663 | 34.5146 | 34.5816 | 34.4983 |
| | FG-O | 16.6984 | 16.6451 | 16.6376 | 17.7250 | 17.6717 | 17.6642 | 27.8571 | 27.8038 | 27.7962 |
| | FG-X | 26.8941 | 27.0177 | 26.8320 | 27.9207 | 28.0443 | 27.8586 | 38.0528 | 38.1764 | 37.9906 |
| 0.17 | UD | 32.3180 | 32.3890 | 32.3051 | 33.3446 | 33.4156 | 33.3316 | 43.4768 | 43.5477 | 43.4637 |
| | FG-O | 22.6823 | 22.6276 | 22.6338 | 22.6823 | 23.6542 | 23.6604 | 33.8410 | 33.7863 | 33.7924 |
| | FG-X | 37.6944 | 37.8069 | 37.6444 | 38.7210 | 38.8335 | 38.6710 | 48.8531 | 48.9656 | 48.8030 |

4.1 收敛性分析

为验证本文方法的收敛性, 采用不同均布节点对单向受压四边简支 FG-CNTRC 方板进行临界屈曲荷载进行分析。CNTs 的分布方式考虑 UD 型、FG-O 型和 FG-X 型 3 种。板的宽厚比为 0.01, 体积分数为 0.11, 相对误差定义为 |本文解 - 文献解| / 文献解 $\times 100\%$, 相关计算结果列入表 3。研究表明, 随着节点数的增多, 数值结果趋于稳定; 当节点数为 17×17 时, 计算结果与 Yang 等^[34] 采用基于一阶剪切变形理论的 Chebyshev-Ritz 方法得到的结果误差在 0.1% 以内, 可认为该离散方案已使计算收敛。

表 3 单压四边简支 FG-CNTRC 方板无量纲临界屈曲荷载

Tab. 3 Dimensionless critical buckling loads of simply supported FG-CNTRC square plate under uniaxial compression

| Method | Type | | |
|--------------------------------|--------------------|--------------------|--------------------|
| | UD | FG-O | FG-X |
| Present(7×7) | 39.3835 (0.05%) | 21.5016 (0.08%) | 57.1058 (0.00%) |
| Present(11×11) | 39.3542 (0.02%) | 21.4735 (0.04%) | 57.0752 (0.05%) |
| Present(15×15) | 39.3468 (0.04%) | 21.4661 (0.07%) | 57.0677 (0.06%) |
| Present(17×17) | 39.3448 (0.04%) | 21.4640 (0.08%) | 57.0656 (0.06%) |
| Present(21×21) | 39.3424 (0.05%) | 21.4617 (0.09%) | 57.0633 (0.07%) |
| Chebyshev-Ritz ^[34] | 39.3633 | 21.483 | 57.1048 |

4.2 有效性分析

为验证本文方法有效性, 根据 4.1 节分析采用无网格节点数 17×17 对厚宽比为 0.1, 不同体积分数下单向受压弹性地基上四边简支 FG-CNTRC 方板的临界屈曲荷载进行分析, 相关计算结果列入表 4。临界屈曲荷载无量纲 $\bar{N}_{cr}^* = N_{cr} b^2 / (\pi^2 D_m)$ 。

由表 4 可知,采用本文方法计算所得结果与 Wattanasakulpong 等^[13]基于 TSDT 和正弦剪切变形理论 SSDT(sinusoidal shear deformation theory),采用 Navier 解答所得的四边简支解析解吻合良好,证明了本文方法求解弹性地基 FG-CNTRC 方板临界屈曲荷载的有效性及准确性。

4.3 参数分析

采用本文方法分析 CNTs 体积分数、分布形式、转向角、板厚宽比及长宽比、地基系数和边界条件对 FG-CNTRC 板临界屈曲荷载的影响。

表 5~表 8 给出了不同地基系数及体积分数下四边简支 FG-CNTRC 方板在单向受压、双向受压、双向拉压及面内剪切下的临界屈曲荷载,板的厚宽比为 0.01。由表 5~表 8 可知,临界屈曲荷载随着地基系数的增加而增大,且地基剪切模量 K_s 比弹性地基模量 K_w 影响剧烈;临界屈曲荷载随着体积分数的增大而增大;FG-X 型分布板的临界屈

表 5 单压四边简支 FG-CNTRC 方板无量纲临界屈曲荷载

Tab. 5 Dimensionless critical buckling loads of simply supported FG-CNTRC square plate under uniaxial compression

| V_{CNT}^* | Type | (k_w, k_s) | | |
|-------------|------|--------------|---------|----------|
| | | (0,0) | (100,0) | (100,50) |
| 0.11 | UD | 39.3448 | 40.2995 | 49.7220 |
| | FG-O | 21.4640 | 22.4187 | 31.8413 |
| | FG-X | 57.0656 | 58.0203 | 67.4428 |
| 0.14 | UD | 49.3860 | 50.3407 | 59.7633 |
| | FG-X | 71.9605 | 72.9152 | 82.3377 |
| 0.17 | UD | 60.4595 | 61.4142 | 70.8367 |
| | FG-X | 88.0272 | 88.9819 | 98.4044 |

表 6 双压四边简支 FG-CNTRC 方板无量纲临界屈曲荷载

Tab. 6 Dimensionless critical buckling loads of simply supported FG-CNTRC square plate under biaxial compression

| V_{CNT}^* | Type | (k_w, k_s) | | |
|-------------|------|--------------|---------|----------|
| | | (0,0) | (100,0) | (100,50) |
| 0.11 | UD | 11.5850 | 11.7759 | 16.4871 |
| | FG-O | 7.8490 | 8.0400 | 12.7512 |
| | FG-X | 14.7470 | 14.8425 | 19.5538 |
| 0.14 | UD | 13.7419 | 13.8941 | 18.6054 |
| | FG-X | 16.8120 | 16.9074 | 21.6187 |
| 0.17 | UD | 17.9676 | 18.1586 | 22.8698 |
| | FG-X | 23.7915 | 23.8870 | 28.5983 |

表 7 拉压四边简支 FG-CNTRC 方板无量纲临界屈曲荷载

Tab. 7 Dimensionless critical buckling loads of simply supported FG-CNTRC square plate under biaxial compression and tension

| V_{CNT}^* | Type | (k_w, k_s) | | |
|-------------|------|--------------|----------|----------|
| | | (0,0) | (100,0) | (100,50) |
| 0.11 | UD | 191.8007 | 192.1189 | 199.9708 |
| | FG-O | 101.3560 | 101.6743 | 109.5262 |
| | FG-X | 278.4596 | 278.7778 | 286.6298 |
| 0.14 | UD | 241.4666 | 241.7848 | 249.6368 |
| | FG-X | 349.6783 | 349.9965 | 357.8484 |
| 0.17 | UD | 294.5982 | 294.9165 | 302.7684 |
| | FG-X | 428.5100 | 428.8282 | 436.6801 |

表 8 面内剪切四边简支 FG-CNTRC 方板无量纲临界屈曲荷载

Tab. 8 Dimensionless critical buckling loads of simply supported FG-CNTRC square plate under in-plane shear

| V_{CNT}^* | Type | (k_w, k_s) | | |
|-------------|------|--------------|----------|----------|
| | | (0,0) | (100,0) | (100,50) |
| 0.11 | UD | 57.0739 | 57.47121 | 68.76951 |
| | FG-O | 36.59352 | 36.99161 | 47.54731 |
| | FG-X | 76.18161 | 76.55555 | 88.16272 |
| 0.14 | UD | 68.20321 | 68.58974 | 80.09163 |
| | FG-X | 90.08144 | 90.33124 | 102.963 |
| 0.17 | UD | 88.38722 | 88.78676 | 100.3337 |
| | FG-X | 119.4809 | 119.8626 | 131.6332 |

表 9 不同厚宽比下单压四边简支 FG-CNTRC 型方板无量纲临界屈曲荷载

Tab. 9 Dimensionless critical buckling loads of simply supported FG-CNTRC square plate under uniaxial compression and different thickness-to-width ratios

| h/b | Type | (k_w, k_s) | | |
|-------|------|--------------|---------|----------|
| | | (0,0) | (100,0) | (100,50) |
| 0.01 | UD | 39.3448 | 40.2995 | 49.7220 |
| | FG-O | 21.4640 | 22.4187 | 31.8413 |
| | FG-X | 57.0656 | 58.0203 | 67.4428 |
| 0.02 | UD | 38.0847 | 39.0394 | 48.4620 |
| | FG-X | 54.4232 | 55.3780 | 64.8005 |
| 0.05 | UD | 31.1845 | 32.1392 | 41.5617 |
| | FG-X | 41.2279 | 42.1826 | 51.6051 |
| 0.1 | UD | 19.2248 | 20.1795 | 29.6020 |
| | FG-X | 22.5323 | 23.4870 | 32.9095 |
| 0.2 | UD | 8.1554 | 9.1101 | 14.4890 |
| | FG-X | 8.6926 | 9.4939 | 14.5431 |

曲荷载最大,FG-O型分布板的临界屈曲荷载最小,UD型分布板介于两者之间,这说明CNTs分布在板的上下表面比分布在板的中面更有利于提高其结构的刚度;双向拉压作用下比双向受压及面内剪切工况下产生更大的临界屈曲荷载;地基系数对不同荷载工况下的临界屈曲荷载影响为面内剪切最大,单向拉压次之,接着是双向拉压,双向受压最小。

表9计算了体积分数为0.11,不同厚宽比下单向受压四边简支FG-CNTRC方板无量纲临界屈曲荷载。由表9可知,随着板宽厚比的增加,横向剪切效应削弱,CNTs的分布方式对临界屈曲荷载的影响将削弱,三类CNTs分布型的方板临界

屈曲荷载数值结果相对差异减小。

图3和图4分别给出了宽厚比为0.01,不用长宽比及边界条件下单向受压四边简支FG-CNTRC板无量纲临界屈曲荷载随体积分数的变化。可以看出,临界屈曲荷载随着长宽比的减少而增大,随着边界条件约束的增强而增大。随着边界条件约束的削弱,临界屈曲荷载-CNTs体积分数增长曲线越加平缓。

图5和6分别讨论了体积分数为0.11,宽厚比为0.1,四边简支或四边固支FG-CNTRC方板在单双压工况下的临界屈曲荷载随CNT转向角变化。从图5(a)和图6(a)可以看出,单向受压四边

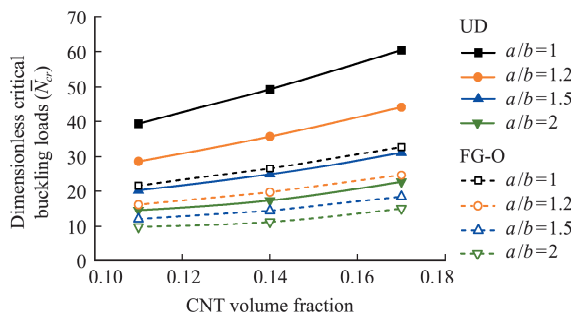


图3 不同长宽比下单压四边简支FG-CNTRC板无量纲临界屈曲荷载随体积分数的变化

Fig. 3 Variation of dimensionless critical buckling loads with CNT volume fraction of simply supported FG-CNTRC plate under uniaxial compression and different length-to-width ratios

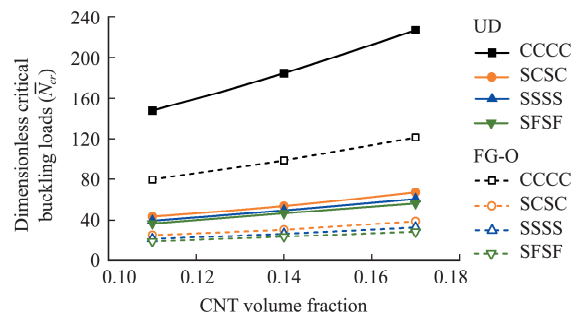
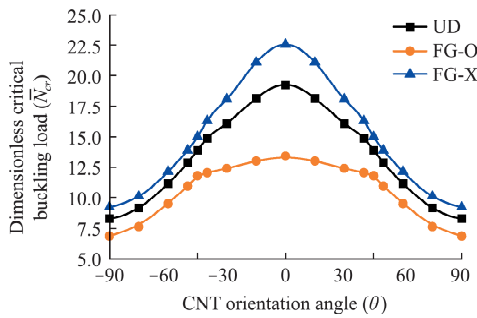
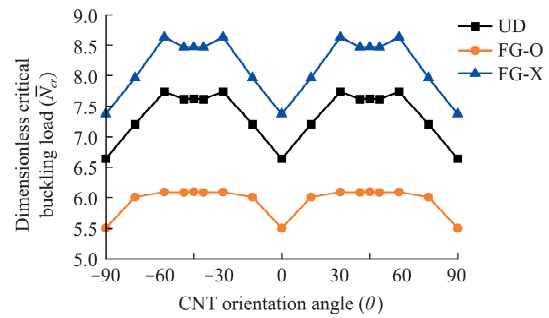


图4 不同边界条件下单压FG-CNTRC方板临界屈曲荷载随体积分数的变化

Fig. 4 Variation of dimensionless critical buckling loads with CNT volume fraction of FG-CNTRC square plate under biaxial compression and different boundary



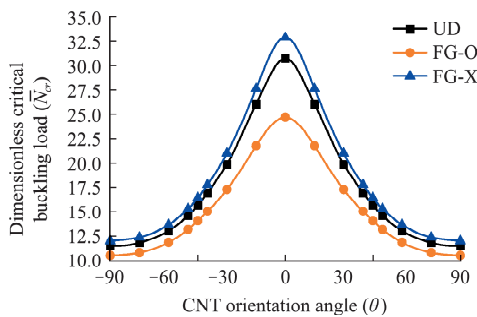
(a) 单压
(a) Uniaxial compression



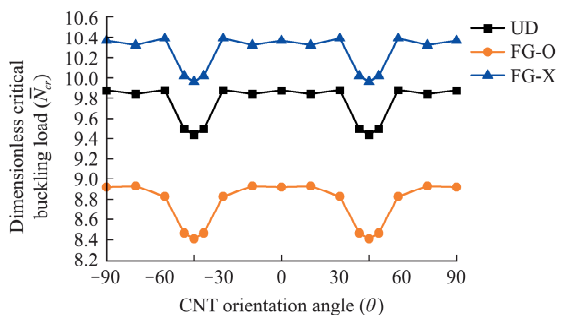
(b) 双压
(b) Biaxial compression

图5 四边简支FG-CNTRC方板临界屈曲荷载随转向角变化

Fig. 5 Variation of dimensionless critical buckling loads with CNT orientation angle of simply supported FG-CNTRC square plate



(a) 单压
(a) Uniaxial compression



(b) 双压
(b) Biaxial compression

图6 四边固支FG-CNTRC方板临界屈曲荷载随转向角变化

Fig. 6 Variation of dimensionless critical buckling loads with CNT orientation angle of clamped FG-CNTRC square plate

简支或四边固支 FG-CNTRC 方板临界屈曲荷载均随着 CNTs 转向角的变化呈现先增后减的规律,转向角 $\theta=0^\circ$ 为最大值且关于 $\theta=0^\circ$ 对称。从图 5(b) 和图 6(b) 可以看出,双向受压四边简支或四边固支 FG-CNTRC 方板临界屈曲荷载-CNTs 转向角变化曲线关于 $\theta=0^\circ$ 对称;四边简支时,临界屈曲荷载在 $\theta=0^\circ$ 和 $\pm 90^\circ$ 达到最小值,在 $\theta=\pm 30^\circ$ 和 $\pm 60^\circ$ 达到最大值;四边固支时,临界屈曲荷载在 $\theta=\pm 45^\circ$ 达到最小值,FG-O 型方板临界屈曲荷载在 $\theta=\pm 15^\circ$ 和 $\pm 75^\circ$ 达到最大值,UD 型及 FG-X 型

方板在 $\theta=0^\circ, \pm 30^\circ$ 和 $\pm 60^\circ$ 达到最大值。以上说明考虑 CNTs 转向以后,加载方式及边界条件等对 FG-CNTRC 方板的临界屈曲荷载影响更为复杂多变。在实际的工况中,要获得更为合理的结构设计需综合考虑各方面参数的影响,进行大量的数值试验。

图 7 给出了体积分数为 0.11,厚宽比为 0.1,不同转向角下单向受压四边简支 UD 型方板的第一阶屈曲模态,可以看出,CNTs 的转向角对模态的影响较为明显。

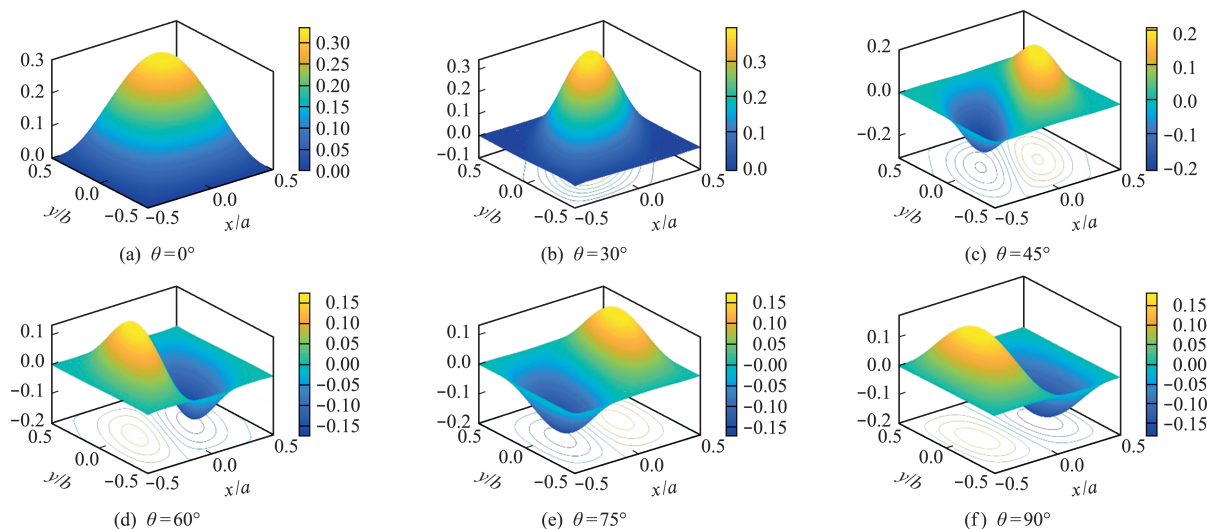


图 7 不同 CNTs 转向角下单压四边简支 UD 型方板第 1 阶屈曲模态

Fig. 7 First order buckling modes of simply supported UD square plate at different orientation angle under uniaxial compression

5 结论

本文基于改进 Reddy 型三阶剪切变形理论,结合移动最小二乘近似,建立了弹性地基上功能梯度碳纳米管增强复合材料板屈曲无网格分析模型。通过基准算例验证了本文方法的收敛性及有效性。研究了 CNTs 的转向角、分布形式、体积率、地基系数边界条件及结构的几何尺寸等因素对临界屈曲荷载的影响,得出如下结论。

(1) FG-CNTRC 板的刚度随着地基系数的增加而增大,地基系数对不同荷载工况下的临界屈曲荷载影响为面内剪切最大,双向拉压次之,接着为单向受压,双向受压最小。

(2) CNTs 的分布形式和体积分数对结构刚度的影响较大,FG-CNTRC 材料形成的结构刚度的大小依次为 $0.17 > 0.14 > 0.11$,FG-X 型 $>$ UD 型 $>$ FG-O 型。

(3) 随着板宽厚比的增加,横向剪切效应削弱,CNTs 的分布方式对临界屈曲荷载的影响将削弱,三类 CNTs 分布型临界屈曲荷载相对差异减小。

(4) FG-CNTRC 板的临界屈曲荷载随着边界条件约束的增强而增大,且随着边界条件约束的削弱,临界屈曲荷载-CNTs 体积分数增长曲线越加平缓。

(5) FG-CNTRC 板的临界屈曲荷载随着转向角的变化曲线呈现一定的规律性,曲线关于 $\theta=0^\circ$ 对称,但其最大/最小值在转向角取何值时出现,需结合荷载及边界条件、分布形式等多方面因素进行综合考虑。

参考文献(References):

- [1] Coleman J N, Khan U, Blau W J, et al. Small but strong: A review of the mechanical properties of carbon nanotube-polymer composites [J]. *Carbon*, 2006, **44**(9): 1624-1652.
- [2] Spitalsky Z, Tasis D, Papagelis K, et al. Carbon nanotube-polymer composites: Chemistry, processing, mechanical and electrical properties [J]. *Progress in Polymer Science*, 2010, **35**(3): 357-401.
- [3] Jafari Mehrabadi S, Sobhani Aragh B, Khoshkhaheh V, et al. Mechanical buckling of nanocomposite rec-

- tangular plate reinforced by aligned and straight single-walled carbon nanotubes [J]. *Composites Part B: Engineering*, 2012, **43**(4): 2031-2040.
- [4] Soltani P. Nonlinear free and forced vibration analysis of a single-walled carbon nanotube using shell model [J]. *International Journal of Fundamental Physical Sciences*, 2011, **1**(3): 47-52.
- [5] Vodenitcharova T, Zhang L C. Bending and local buckling of a nanocomposite beam reinforced by a single-walled carbon nanotube [J]. *International Journal of Solids and Structures*, 2006, **43**(10): 3006-3024.
- [6] 李煜冬, 傅卓佳, 汤卓越. 功能梯度碳纳米管增强复合材料板弯曲和模态的广义有限差分法 [J]. *力学学报*, 2022, **54**(2): 414-424. (LI Yu-dong, FU Zhuo-jia, TANG Zhuo-chao. Generalized finite difference method for bending and modal analysis of functionally graded carbon nanotube-reinforced composite plates [J]. *Chinese Journal of Theoretical and Applied Mechanics*, 2022, **54**(2), 414-424. (in Chinese))
- [7] 薛婷, 秦现生, 张顺琦, 等. 基于一阶剪切变形理论的 CNTRC 板的自由振动分析 [J]. *机械工程学报*, 2019, **55**(24): 45-50. (XUE Ting, QIN Xian-sheng, ZHANG Shun-qi, et al. Free vibration analysis of CNTRC plates based on first-order shear deformation theory [J]. *Journal of Mechanical Engineering*, 2019, **55**(24): 45-50. (in Chinese))
- [8] 薛婷, 秦现生, 张顺琦, 等. 碳纳米管增强功能梯度复合材料薄板建模与分析 [J]. *机械工程学报*, 2018, **54**(16): 93-100. (XUE Ting, QIN Xian-sheng, ZHANG Shun-qi, et al. Geometrically linear modeling and analysis of functionally graded carbon nanotube-reinforced composite rectangular plates [J]. *Journal of Mechanical Engineering*, 2018, **54**(16): 93-100. (in Chinese))
- [9] Shen H S. Nonlinear bending of functionally graded carbon nanotube-reinforced composite plates in thermal environments [J]. *Composite Structures*, 2009, **91**(1): 9-19.
- [10] Shen H S, Zhang C L. Thermal buckling and post buckling behavior of functionally graded carbon nanotube-reinforced composite plates [J]. *Materials & Design*, 2010, **31**(7): 3403-3411.
- [11] Yas M H, Samadi N. Free vibrations and buckling analysis of carbon nanotube-reinforced composite Timoshenko beams on elastic foundation [J]. *International Journal of Pressure Vessels and Piping*, 2012, **98**: 119-128.
- [12] Wattanasakulpong N, Ungbhakorn V. Analytical solutions for bending, buckling and vibration responses of carbon nanotube-reinforced composite beams resting on elastic foundation [J]. *Computational Materials Science*, 2013, **71**: 201-208.
- [13] Wattanasakulpong N, Chaikittiratana A. Exact solutions for static and dynamic analyses of carbon nanotube-reinforced composite plates with Pasternak elastic foundation [J]. *Applied Mathematical Modelling*, 2015, **39**(18): 5459-5472.
- [14] Zhang L W, Lei Z X, Liew K M. An element-free IMLS-Ritz framework for buckling analysis of FG-CNT reinforced composite thick plates resting on Winkler foundations [J]. *Engineering Analysis with Boundary Elements*, 2015, **58**: 7-17.
- [15] 王冰冰. 高阶无网格法的节点积分及薄板壳力学分析 [D]. 大连理工大学, 2018. (WANG Bing-bing. Node Integration of Higher-Order Meshless Method and Mechanical Analysis of Thin Plates and Shells [D]. Dalin University of Technology, 2018. (in Chinese))
- [16] 李迪. 板壳畸变单元的无网格和有限元自适应耦合方法研究 [D]. 上海交通大学, 2009. (LI Di. Research on Adaptive Coupling Method of Meshless and Finite Element for Distorted Element of Plate and Shell [D]. Shanghai Jiao Tong University, 2009. (in Chinese))
- [17] Lei Z X, Liew K M, Yu J L. Large deflection analysis of functionally graded carbon nanotube-reinforced composite plates by the element-free kp-Ritz method [J]. *Computer Methods in Applied Mechanics and Engineering*, 2013, **256**: 189-199.
- [18] Lei Z X, Liew K M, Yu J L. Buckling analysis of functionally graded carbon nanotube-reinforced composite plates using the element-free kp-Ritz method [J]. *Composite Structures*, 2013, **98**: 160-168.
- [19] Lei Z X, Liew K M, Yu J L. Free vibration analysis of functionally graded carbon nanotube-reinforced composite plates using the element-free kp-Ritz method in thermal environment [J]. *Composite Structures*, 2013, **106**: 128-138.
- [20] Zhang L W, Lei Z X, Liew K M. Free vibration analysis of functionally graded carbon nanotube-reinforced composite triangular plates using the FSDT and element-free IMLS-Ritz method [J]. *Composite Structures*, 2015, **120**: 189-199.
- [21] 彭林欣. 折板结构非线性弯曲分析的移动最小二乘无网格法 [J]. *工程力学*, 2011, **28**(12): 126-132. (PENG Lin-xin. Nonlinear bending analysis of folded plate structures by the moving-least square meshfree method [J]. *Engineering Mechanics*, 2011, **28**(12): 126-132. (in Chinese))
- [22] 杨健生, 曾治平, 韦冬炎, 等. 基于无网格法的非均匀弹性地基上变厚度加筋板弯曲与固有频率分析 [J]. *计算力学学报*, 2021, **38**(3): 364-370. (YANG Jian-sheng, ZENG Zhi-ping, WEI Dong-yan, et al. Bending and natural frequency analysis of variable thickness stiffened plates on non-uniform elastic foundation based on meshless method [J]. *Chinese Journal of Computational Mechanics*, 2021, **38**(3): 364-370. (in Chinese))
- [23] Hosseini S, Rahimi G, Anani Y. A meshless collocation method based on radial basis functions for free

- and forced vibration analysis of functionally graded plates using FSDT [J]. *Engineering Analysis with Boundary Elements*, 2021, **125**:168-177.
- [24] Vu T V, Nguyen N H, Khosravifard A, et al. A simple FSDT-based meshfree method for analysis of functionally graded plates [J]. *Engineering Analysis with Boundary Elements*, 2017, **79**:1-12.
- [25] Selim B A, Zhang L W, Liew K M. Vibration analysis of CNT reinforced functionally graded composite plates in a thermal environment based on Reddy's higher-order shear deformation theory [J]. *Composite Structures*, 2016, **156**:276-290.
- [26] Reddy J N. A simple higher-order theory for laminated composite plates [J]. *Journal of Applied Mechanics*, 1984, **51**(4):745-752.
- [27] Selim B A, Zhang L W, Liew K M. Active vibration control of FGM plates with piezoelectric layers based on Reddy's higher-order shear deformation theory [J]. *Composite Structures*, 2016, **155**:118-134.
- [28] Selim B A, Zhang L W, Liew K M. Active vibration control of CNT-reinforced composite plates with piezoelectric layers based on Reddy's higher-order shear deformation theory [J]. *Composite Structures*, 2017, **163**:350-364.
- [29] Zhang L W, Selim B A. Vibration analysis of CNT-reinforced thick laminated composite plates based on Reddy's higher-order shear deformation theory [J]. *Composite Structures*, 2017, **160**:689-705.
- [30] Memar Ardestani M, Zhang L W, Liew K M. Isogeometric analysis of the effect of CNT orientation on the static and vibration behaviors of CNT-reinforced skew composite plates [J]. *Computer Methods in Applied Mechanics and Engineering*, 2017, **317**:341-379.
- [31] Pasternak P L. On a new method of an elastic foundation by means of two foundation constants [J]. *Gosudarstvennoe Izdatelstvo Literaturi Po Stroitelstve I Arkhitekture*, 1954.
- [32] Lancaster P, Salkauskas K. Surfaces generated by moving least squares methods [J]. *Mathematics of Computation*, 1981, **37**(155):141-158.
- [33] Chen J S, Pan C H, Wu C T, et al. Reproducing Kernel Particle Methods for large deformation analysis of non-linear structures [J]. *Computer Methods in Applied Mechanics and Engineering*, 1996, **139**(1-4):195-227.
- [34] Yang J, Chen D, Kitipornchai S. Buckling and free vibration analyses of functionally graded graphene reinforced porous nanocomposite plates based on Chebyshev-Ritz method [J]. *Composite Structures*, 2018, **193**:281-294.

Meshless buckling analysis of FG-CNTRC plate on elastic foundation based on improved Reddy type third-order shear deformation theory

XU Jian-wen¹, YAN Shi-tao², PENG Lin-xin³, CHEN Wei^{*3,4}

(1. Guangxi Xinfazhan Communication Group Co., Ltd., Nanning 530004, China;

2. Guangxi Transport Vocational and Technical College, Nanning 530004, China;

3. School of Civil Engineering and Architecture, Guangxi University, Nanning 530004, China;

4. School of Civil Engineering, University of South China, Hengyang 421001, China)

Abstract: In order to solve the buckling problem of functionally graded carbon nanotube reinforced composite (FG-CNTRC) plates with carbon nanotubes (CNTs) orientation angle resting on an elastic foundation, a meshless analysis model based on improved Reddy's third-order shear deformation theory (TSDT) and moving least square (MLS) is proposed. This model avoids the difficulty of imposing the second kind of boundary condition in the meshless method, and can satisfy the free surface conditions of medium thick/thick plates without introducing additional shear correction factors. Based on the principle of minimum potential energy, the governing meshless equations for the buckling of FG-CNTRC plates on an elastic foundation are derived. The convergence and effectiveness of this method are verified by a benchmark example. The effects of the orientation angle, volume fraction, distribution pattern, foundation coefficient, width-to-thickness ratio and boundary condition on the critical buckling loads of FG-CNTRC plates are analysed.

Key words: improved Reddy's third-order shear deformation theory; functionally graded carbon nanotube reinforced composite plate; Pasternak foundation; critical buckling load; moving-least square approximation